Plasma properties near the anode surface of an ion diode determined by high-resolution laser spectroscopy

L. Perelmutter,* G. Davara, and Y. Maron
Department of Physics, Weizmann Institute of Science, Rehovot, Israel
(Received 10 January 1994)

Techniques based on resonant absorption and induced fluorescence for the determination of densities and velocity distributions of ions and atoms in the vicinity of a surface in contact with a plasma were developed. Using these techniques, densities and velocity distributions were obtained for various species at distances down to about 30 μm from the anode surface in an ion diode. Singly charged ions were observed to acquire kinetic energies of about 15 eV within 30 μm from the surface, indicating an average accelerating electric field of 5 kV/cm in this region. For the relatively fast ionizing particles, the density gradients due to ionizations at such distances were observed. These data and the observed H_α absorption profile are used to estimate the electron density and temperature and the absolute particle fluxes close to the anode surface. We believe such measurements can be useful in studying various phenomena near plasma-wall interfaces.

PACS number(s): 52.40.Hf, 52.75.Pv, 52.25.Qt, 52.70.Kz

I. INTRODUCTION

Experimental studies of densities and velocity distributions of ions or atoms and of the charge state distributions in plasmas in the immediate vicinity of surfaces is important for investigations of various plasma-wall interactions such as electrode phenomena in electrical discharges, plasma formation in plasma sources for various applications, material ejection from surfaces into plasmas, plasma-assisted manufacturing, and plasma sheaths. For such studies, nonintrusive measurements of high spatial and temporal resolutions should be developed.

In previous studies [1,2], we determined the velocities and absolute densities of various species in a 1-mm-wide anode plasma formed over the dielectric anode surface in a planar magnetically insulated ion diode. Those measurements utilized spectral profiles and absolute intensities of spontaneous emission lines that, together with the electron density observed from Stark broadening and time-dependent collisional radiative calculations, gave the densities and velocities of various species in the anode plasma. These measurements, performed for distances $\gtrsim 200$ μm from the anode surface, could not be extended to regions closer to the surface because of the following reasons. First, with spontaneous emission, it is difficult to achieve a spatial resolution of tens of micrometers since it is difficult to avoid light collected from a wider region of the plasma. Also, the electron density and temperature at such distances from the surface are difficult to obtain. This hinders the use of collisional-radiative calculations to determine the ground-state densities from the observed excited-level densities, while in such experiments in rapidly ionizing plasmas most of the particles (atoms or ions) are in their ground states [3]. Furthermore, collisional-radiative modeling in the immediate vicinity of the surface may be unreliable because of the usually unknown continuous particle ejection from the surface. This material ejection particularly affects the excited- to ground-state density ratio because of the lack of sufficient time for equilibrium within each charge state. Finally, spontaneous emission measurements near surfaces can be strongly affected by limited light collection efficiency due to the neighboring surface, and by opacity effects due to the relatively high particle densities there.

In this study, we developed a method based on laser light resonant absorption to determine the ground-state densities of atoms and singly charged ions within down to 30 μm from the surface. With this method, uncertainties due to self-absorption effects are avoided, and the ground-state densities are determined directly, without the use of collisional-radiative calculations. In addition, absolute calibration of the detection system is not required since the level densities are determined from relative absorption measurements. Furthermore, while with spontaneous emission the measurements integrate along the line of sight, with the method developed in this study the densities could be determined at selected regions of the surface by limiting the interaction region of the laser light and the absorbing particles.

Using resonant absorption and induced-fluorescence measurements we determined the densities of H I, Li I, and Mg II in the anode plasma as a function of distance from the anode surface (the presence of Li I and Mg II in the plasma was due to adding compounds of lithium and magnesium to the anode dielectric). For Li I and Mg II, density gradients much higher than for H I where seen within 50 μm from the anode surface. This could be explained by the ionization of Li I and Mg II ejected from the anode surface during their motion away from the surface. The particle velocities were determined from the

*Present address: NRC Soreq, Yavne 81800, Israel.

Doppler broadenings of the absorption lines. These measurements indicated that the ions acquire most of their kinetic energies seen in the anode plasma (about 15 eV for singly charged ions) within 30 μm from the anode surface. This implies effective electric fields of 5 kV/cm in this region. It is also consistent with our previous conclusion [1,2], based on velocity measurements for various charge-state ions, that the ions are accelerated in the immediate vicinity of the surface.

Using the observed particle velocities and densities, particle ionization times within 50 μm from the surface were estimated. This gave bounds on the electron density and temperature in this region near the surface [4]. We also observed the H_α absorption profile in this region. From the contribution of the Stark broadening to the H_α width, we obtained an upper bound for the electron density, which is found to be consistent with that obtained from the particle ionizations. A detailed analysis of the data for the determination of the electron density and temperature at this distance from the anode surface will be given in a subsequent publication. Finally, the absolute particle fluxes into the plasma averaged over $\simeq 30$ μm from the surface were obtained.

II. THE EXPERIMENTAL ARRANGEMENT

The plasma in these experiments was produced via a flashover of a dielectric-anode surface in a planar magnetically insulated gap, the details of which are described in Ref. [1]. A diagram of the experimental system is given in Fig. 1(a). The diode was powered by a 270-kV, 90-ns pulse produced by a LC-waterline generator and the magnetic field used to inhibit the electron flow across the 8-mm-wide diode gap was $B_z = 7$ kG. The diode-voltage wave form is given in Fig. 1(b).

The dye laser used in these experiments is pumped by a Q-switched Nd:YAG (yttrium aluminum garnet) laser and is equipped with doubling and mixing crystals that allow for wavelength tuning down to 2160 Å. The light pulse was $\simeq 6$ ns long, and its application time during the high-voltage pulse was varied in the experiments. The laser beam could be directed into the anode plasma in various directions. Cylindrical lenses were used to determine the beam shape in the observation region.

The laser beam power was measured in each discharge by reflecting a small fraction of the laser beam onto a calibrated fast photodiode. In order to obtain an absorp-

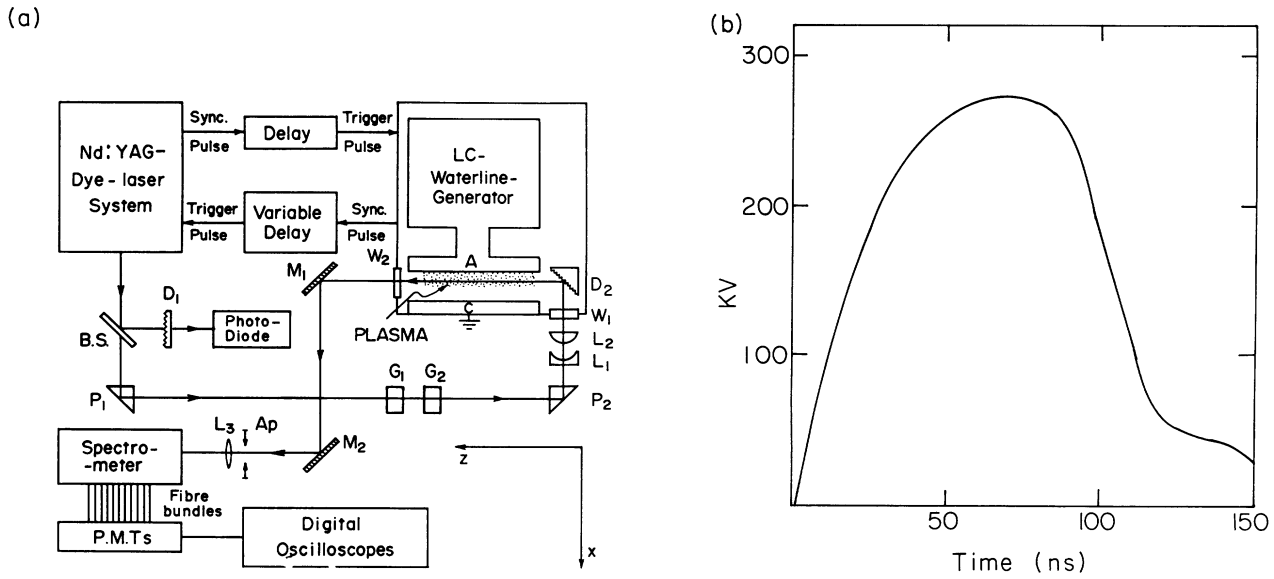

FIG. 1. (a) Schematic illustration of the experimental system. Shown are the anode (A) and cathode (C) of a planar diode insulated by an externally applied magnetic field B_z parallel to the electrodes. The diode is powered by an LC-waterline generator. The Nd:YAG dye laser system is synchronized with the LC-waterline generator by a variable delay circuit. The laser beam can be directed into the anode plasma in various directions. In the one shown here, the beam is directed via prisms (P_1 and P_2) and a telescope made of cylindrical lenses (L_1 and L_2). The laser light is scattered from a diffuser (D_2) mounted on the shank behind the anode stalk, and then passes through the plasma in the z direction to the spectroscopic detection system. A small fraction of the laser light reflected by a beam splitter (BS) is recorded by a fast photodiode to give the laser pulse power and time. Attenuation of the laser beam and rotation of its vector of polarization are made by two glan-laser air-spaced prism polarizers (G_1 and G_2). Light from the plasma (transmitted laser light, spontaneous emission, or laser induced fluorescence) is focused on the spectrometer entrance slit using mirrors (M_1 and M_2) and a lens (L_3). The observation distance from the anode surface is varied in the experiments by displacing mirror M_2. The angle of view of the lens L_3 was reduced down to 2.5 mrad in the x direction by using a rectangular aperture (A_p) mounted in front of the lens. The light at the spectrometer exit window is optically further dispersed, and the spectral line profile is then sampled by a set of 11 optical fiber bundles that transmit the light to a set of 11 photomultiplier tubes (PMT's), the signals of which are recorded by digital oscilloscopes, giving the light spectral profile as a function of time in a single discharge. (b) The diode-voltage wave form.

tion spectral profile in a single discharge, as described below, the spectral width of the laser light was set to be a little larger than the absorption line.

The spectroscopic detection system is shown in Fig. 1(a), and was described in Ref. [1]. Here, in order to improve the spatial resolution in the x direction, the solid angle of the light collection system was reduced down to 2.5 mrad in this direction by using a rectangular aperture. In order to observe the line spectral profile in a single discharge, the light at the spectrograph exit was further optically dispersed and projected onto a rectangular 11-channel optical-fiber array. The light transmitted by each channel was measured by a photomultiplier tube and an oscilloscope, giving 11 time-dependent data points of the spectral profile.

The anode used in our experiments is described in Fig. 2. The length and height of the epoxy-filled grooved aluminum plate (the active anode) were $L_z=13$ cm and $L_y=6.5$ cm, respectively. The relatively long active anode ($L_z=13$ cm) allowed for nearly planar geometry for the diode. In order to limit the laser-particle interaction to the central part of the anode, a region with dimensions $l_z=4$ cm and $l_y=5$ cm at the anode center was elevated by 0.5 mm, and compounds (MgF_2, $AlNaSiO_3$, CaF_2, LiF, and BaF_2) of the elements interacting with the laser light were mixed with the epoxy only in this region. It was ascertained that particles ejected during the pulse from other parts of the anode, as a result of contamination of the entire anode during the discharges, remained within <0.5 mm from the anode surface and, therefore, did not interact with the laser light. The length l_z of the elevated region was so chosen to be within the depth of focus of the detection system, and to allow for a laser light absorption that yields the maximum measurement accuracy (see Sec. III). In order to obtain a uniform plasma in the y direction, which was particularly required for the absorption measurements, the elevated region was made of flat epoxy with no aluminum grooves.

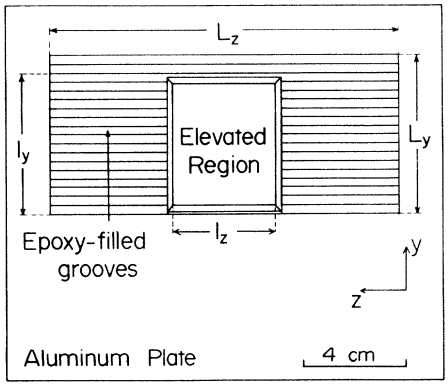

FIG. 2. The anode geometry. The length and height of the active anode region are L_z and L_y, respectively. Most of that region consists of epoxy-filled aluminum grooves. A central part of the anode with length and height l_z and l_y, respectively, is elevated by 0.5 mm and is made of a flat epoxy sheet (with no grooves). The epoxy in the elevated region was mixed with powders of MgF_2, $AlNaSiO_3$, CaF_2, LiF, and BaF_2. Using this geometry the laser light was absorbed only by particles over the elevated region.

III. MEASUREMENTS AND RESULTS

A. Densities of atoms and ions at distances $\gtrsim 50$ μm from the anode surface

In this section we describe the procedure used to determine the absolute level densities of different species in the plasma at distances $\gtrsim 50$ μm from the anode surface, by the use of laser absorption. Here we use our data to calculate the density ratio of the Mg II ground state to the $3p\ ^2P_{3/2}$ level. We also describe the determination of the density ratio of these Mg II levels using saturated laser induced fluorescence. The absolute level densities of the different species in the plasma are given in Sec. III B 1.

The absorption measurements were performed for the Mg II $3s\rightarrow 3p\ ^2P_{3/2}$ (2796 Å), Mg II $3p\ ^2P_{3/2}\rightarrow 3d$ (2798 Å), hydrogen $n=2\rightarrow n=3$ (6563 Å), and Li I $2s\rightarrow 2p$ (6708 Å) transitions. In these measurements, aimed to determine the particle densities at distances $\gtrsim 50$ μm from the anode surface, the laser light was scattered from a diffuser mounted on the anode stalk and passed through the plasma in the z direction, as shown in Fig. 3(a). The

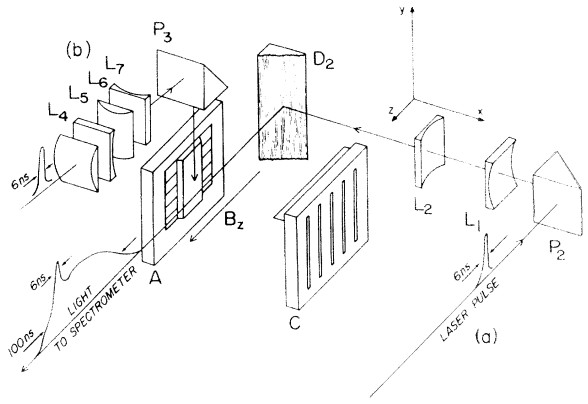

FIG. 3. Illustration of the two optical arrangements used for the laser beam. (a) The laser beam is directed into the diode using a prism (P_2) and cylindrical lenses (L_1,L_2), and is scattered from a diffuser (D_2) mounted on the shank behind the anode stalk (A). The light then passes through the plasma in the z direction toward the detection system as shown in Fig. 1(a). This arrangement was used for absorption measurements at distances $\gtrsim 50$ μm from the anode surface (see text). (b) The laser beam is directed by cylindrical lenses (L_4-L_7) and a prism (P_3) into the plasma in the $-y$ direction. This arrangement is used either to induce fluorescence in the anode plasma by directing the laser beam parallel to the anode, or to make it impinge on a small section of the elevated anode surface. In the latter case, the light scattered from the diffuse surface and passing through the plasma in the z direction is collected by the detection system. The latter arrangement was used for absorption measurements within $\simeq 30$ μm from the anode surface (see text).

spectral profile of the light transmitted through the plasma was observed. An example of such a profile for the Mg II $3s \rightarrow 3p\ ^2P_{3/2}$ transition is shown in Fig. 4. In order to obtain the net spectral profile of the transmitted laser light, the spontaneous emission profile had to be subtracted from the observed profile. The spontaneous emission intensity during the laser pulse was determined by interpolation of the intensities before and after the laser pulse. This procedure introduced no significant error since the spontaneous emission intensity varied little during the laser-pulse duration.

The true line spectral profile, deconvolved from the measured spectral profile of the transmitted laser light using the spectral instrumental response, was used to obtain the absorption coefficient $\alpha(\lambda)$. Gaussian curves were found to fit most of the data satisfactorily, giving the total absorption coefficients $\alpha(\lambda_0)$ at the line centers and the absorption line full widths (σ_{FWHM}) for the different species.

In order to determine the density N_l of the lower level of the transition, we use the formula

$$N_l = \frac{\alpha(\lambda_0)\sigma_{\mathrm{FWHM}}}{p_0 f_{lu} \lambda_0^2} + N_u \frac{g_l}{g_u} , \tag{1}$$

where σ_{FWHM} is in Å, $p_0 = 8.3 \times 10^{-21}$ cm^2/Å for a Gaussian and 5.65×10^{-21} cm^2/Å for a Lorentzian, f_{lu} is the absorption oscillator strength, λ_0 is the wavelength in Å at the line center, densities are in cm^{-3}, and $\alpha(\lambda_0)$ is in cm^{-1}. In Eq. (1), the second term on the right-hand side, which accounts for the stimulated emission, is proportional to the upper level density N_u. Therefore, for example, for the determination of the Mg II ground-state density, the Mg II $3p\ ^2P_{3/2}$ level density, or the density ratio for this level and the Mg II ground state ($3s$) have to be determined independently.

We now describe the determination of the densities of the Mg II ground state and $3p\ ^2P_{3/2}$ level, and we calculate the density ratio for these levels. First, the $3p\ ^2P_{3/2}$ level density was determined by performing resonant absorption measurements for the $3p\ ^2P_{3/2} \rightarrow 3d$ transition. For this determination, knowledge of the density ratio of the $3d$ and $3p\ ^2P_{3/2}$ is also required, again in order to account for the stimulated emission term in Eq. (1). The latter ratio was determined from the spontaneous-emission intensity ratio of the $3p\ ^2P_{3/2} \rightarrow 3s$ and the $3d \rightarrow 3p\ ^2P_{3/2}$ transitions. The stimulated emission term in Eq. (1) was thus accounted for in determining the densities of both the $3s$ and $3p\ ^2P_{3/2}$ levels. For our parameters, because of the higher density of the ground state, the relative contribution of the stimulated emission term for the various species studied was small and ranged between 7 and 20%. Note that the straightforward determination of the lower level density, as given in Eq. (1), requires that the laser light intensity is low enough to negligibly affect the populations of the levels involved, which was ascertained in our experiments. The density ratio of the Mg II ground state to the $3p\ ^2P_{3/2}$ level thus obtained was found to be 3 ± 1 for $x = 250\ \mu$m.

The Mg II ground-state density was also determined using saturated laser-induced fluorescence. Here the laser beam was directed in the $-y$ direction and the induced fluorescence was collected in the z direction, as shown in Fig. 3(b). The laser was tuned to induce the Mg II $3s \rightarrow 3p\ ^2P_{3/2}$ transition (2795.5 Å). In these measurements the laser pulse power per unit area was approximately 70 kW/cm^2, experimentally verified to be sufficient for saturating the excitation. The laser beam was linearly polarized in the z direction. Using a trap for the laser light at the bottom of the diode, the scattered laser light was reduced to 3% of the measured fluorescence intensity. In order to ensure uniform excitation of the Mg II ions, the anode region at which the MgF_2 compound was mixed with the epoxy was 0.7 cm long in the z direction, shorter than the laser beam width ($\simeq 2$ cm) in this direction.

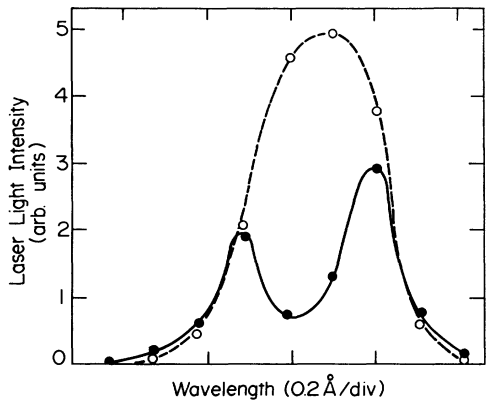

FIG. 4. A typical spectral profile of the laser light transmitted through the plasma (solid curve) and with no plasma in the diode (dashed curve). The laser light wave length is $\lambda \simeq 2795.5$ Å, the center of the Mg II $3s \rightarrow 3p\ ^2P_{3/2}$ transition. The curves indicate the trend. The dip in the solid curve is due to resonant absorption of the laser light in the plasma (see text).

The resulting fluorescence of the $3p\ ^2P_{3/2} \rightarrow 3s$ transition is shown in Fig. 5(a). The signal shown was taken from a measurement at the wavelength corresponding to half the maximum of the observed line profile, where the self-absorption effect is small. Still using the $3s \rightarrow 3p\ ^2P_{3/2}$ excitation, we also observed the fluorescence of the $3p\ ^2P_{1/2} \rightarrow 3s$ transition. As seen in Fig. 5(b) the maximum fluorescence signal observed in this measurement was approximately a factor $\simeq 1.9$ higher than the spontaneous emission. This means that a significant fraction of the Mg II ions, excited to the $3p\ ^2P_{3/2}$ level are deexcited to the $3p\ ^2P_{1/2}$ level during the laser pulse. Calculations of electron-collision transitions between these two levels for the electron density and temperature considered (see Sec. IV) appear to be consistent with this finding [5].

Thus, under the excitation saturation and the collision transitions between the $3p$ levels, we obtain

$$\frac{N_{3s}}{N_{3p}} = \frac{I_{\mathrm{fl}}}{I_{\mathrm{sp}}} \left[\frac{g_{3s}}{g_{3p}} + 1 \right] - 1 , \tag{2}$$

where I_{fl} is the total measured fluorescence intensity cor-

responding to the $3p \rightarrow 3s$ transitions, I_{sp} is the spontaneous emission corresponding to the same transitions with no laser application, and g_{3s} and g_{3p} are the degeneracies of the $3s$ and $3p$ levels, respectively. I_{sp} is obtained in the same discharge from interpolation of the emission before and after the laser pulse.

In Eq. (2) we assumed that the total density of the $3s$ and $3p$ levels remains constant during the laser pulse. However, our collisional-radiative calculations indicate that the total density decreases due to ionizations by $\simeq 15\%$, which was accounted for in the determination of our error. Also, the response time of our detection system, being comparable to the laser-pulse duration, was found to reduce the apparent rise of the intensity due to the fluorescence, by a factor of 2.2, which was corrected for in our data analysis [6].

The ratio of the ground-state density to that of the excited state, $3p\ ^2P_{3/2}$, obtained from the fluorescence measurements, was found to be $\simeq 3.5 \pm 1$, in agreement with the ratio obtained from the absorption measurements. The uncertainty in the above ratio mainly results from uncertainties in the saturation of the excitation, in the $3p\ ^2P_{3/2}$ deexcitation into the $3p\ ^2P_{1/2}$ level during the laser pulse, and in the time response of our detection system.

Our procedure to determine the level density ratios using the fluorescence measurements was experimentally examined by using the same procedure to determine the $3p\ ^2P_{3/2}$ and $4s$ density ratio. We tuned our laser to induce the $3p\ ^2P_{3/2} \rightarrow 4s$ transition and the density ratio for these levels was determined using Eq. (2). It was found to agree with that obtained from the $4s \rightarrow 3p\ ^2P_{3/2}$ and the $3p\ ^2P_{3/2} \rightarrow 3s$ spontaneous-emission intensities, confirming the fluorescence measurements.

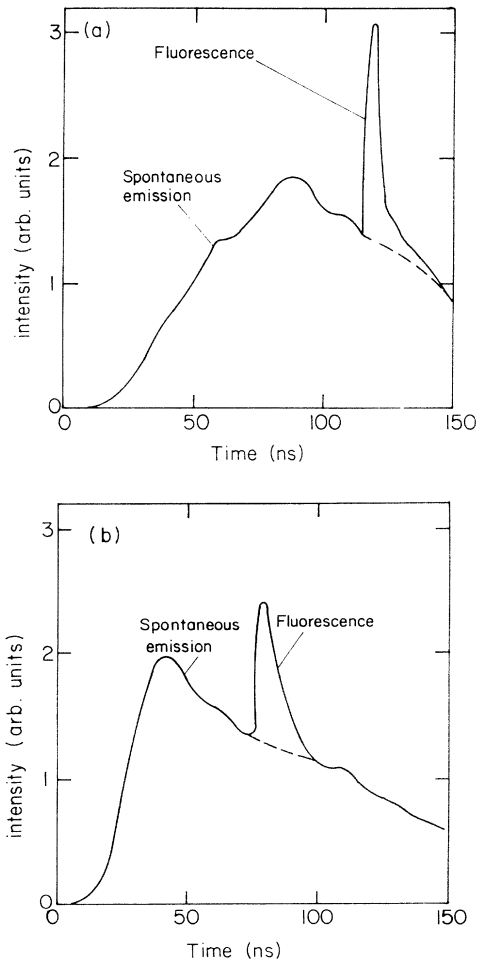

FIG. 5. (a) Spontaneous emission and induced fluorescence of the Mg II $3p\ ^2P_{3/2} \rightarrow 3s$ transition, with a laser excitation of the $3s \rightarrow 3p\ ^2P_{3/2}$ transition. Here the laser power per unit area was $\simeq 70$ kW/cm^2, the time was $\simeq 120$ ns after the start of the high voltage pulse, and the observation distance from the anode surface, and the spatial resolution were both $\simeq 100$ μm. The laser-induced fluorescence signal shown was corrected for the effect of the relatively long response time of the light detection system in order to obtain the true peak intensity of the fluorescence signal (see text). (b) Spontaneous emission and induced fluorescence of the Mg II $3p\ ^2P_{1/2} \rightarrow 3s$ transition, with the same excitation as in (a). Here the laser power per unit area was $\simeq 800$ kW/cm^2, the time was $t \simeq 80$ ns, and the observation distance from the anode surface and the spatial resolution were $\simeq 100$ μm.

B. Densities and velocities at distances < 50 μm from the anode surface

1. *Densities of ground and excited states*

For these measurements, in which resonant laser absorption was used, the laser beam was directed nearly in the $-y$ direction [see Fig. 3(b)], at an angle $\simeq 15$ mrad with the anode surface, to illuminate a rectangular portion of the elevated anode region that is shown in Fig. 2. The dimensions of the illuminated region were 5 cm and 1–4 mm in the y and z directions, respectively. Light was collected from a region 15-mm high (in the y direction) at the anode center. Laser light scattered from the surface and transmitted through the plasma in the z direction was collected within an angle of $\simeq 2.5$ mrad in the x-z plane. The path length in the plasma of the collected laser light was varied in the experiments by moving the spot of the impinging laser beam along the z axis, allowing the laser light attenuation as a function of the path length to be measured.

The optical depth at the line center of the $3s \rightarrow 3p\ ^2P_{3/2}$ transition, as a function of Δz, where Δz is the distance between the laser spot on the anode and the edge of the elevated anode region, is given in Fig. 6. As seen in Fig. 6, the optical depth increases linearly as a function of Δz, as expected for attenuation due to a uniform distribution of the absorbing Mg II ions near the surface of the anode elevated region. Also seen in Fig. 6 is that the linear dependence crosses the Δz axis close to $\Delta z = 0$, confirming that the absorption occurs due to interaction with Mg II ions mainly in the elevated anode region, as stated in Sec. II. This observation also shows that the laser beam absorption in the beam path in the

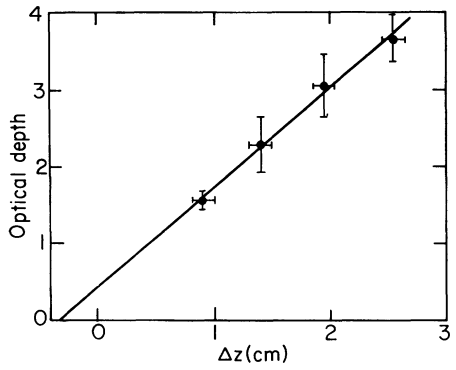

FIG. 6. The measured optical depth as a function of the laser light path length Δz in the plasma in the z direction for $\lambda \simeq 2795.5$ Å, the center of the Mg II $3s \rightarrow 3p\ ^2P_{3/2}$ transition. In the graph, the optical depth is normalized to the average spectral linewidth, $\sigma_{FWHM}=0.2$ Å, observed. The time is $t \simeq 165$ ns. The straight line is a least-square fit to the data.

$\simeq -y$ direction is negligibly small. This results from the short length of the laser beam path in the $-y$ direction in the dense plasma close to the anode surface, and from the saturation of the absorption along the beam path in this direction caused by the relatively high laser beam intensity. Therefore, in determining the particle densities we only accounted for absorption of the scattered light as it propagates in the z direction from the illuminated portion of the anode to the edge of the elevated region.

The high spatial resolution of $\simeq 30$ μm achieved in these measurements resulted mainly from the use of the anode surface as a secondary light source, and from collecting the light from the surface at a sufficiently small angle. The maximum distance from the surface at which the light absorption occurs is given approximately by the path length of the light along the elevated region, ranging from 0.9 to 2.5 cm in the different measurements, times the collection angle of the detection system in these measurements (2.5 mrad). The highest spatial resolution was therefore obtained using the minimum light path length along the elevated region (0.9 cm). Together with the surface roughness, measured to be $\simeq \pm 10$ μm, the highest spatial resolution thus achieved was $\simeq 30$ μm.

With this method we determined the densities of the Mg II $3s$ and $3p\ ^2P_{3/2}$ levels within $\simeq 30$ μm from the anode surface. We employed absorption and emission measurements and data analysis for all the transitions described in Sec. III A.

The measured densities as a function of distance from the anode surface of the Mg II ground ($3s$) and excited ($3p\ ^2P_{3/2}$) states are shown in Fig. 7. The data point closest to the surface is at $x=15$ μm, since it represents an average over the 30-μm-wide region near the surface. It is obtained from the absorption of the laser light scattered on the anode surface, as described in this section. The data points for $x \geq 50$ μm were obtained from the absorption measurements described in Sec. III A.

Using the collisional-radiative calculations for a wide range of electron temperatures and densities, we found that most of the Mg II ions lie in the $3s$ and $3p$ levels. The density gradients shown in Fig. 7 reveal, therefore, a large gradient in the Mg II total density near the anode surface.

It is instructive to show the limitation of the use of spontaneous emission for measurements at such small distances from the surface. In Fig. 7(b) the Mg II $3p\ ^2P_{3/2}$ level density is shown together with the observed emission intensity of the $3p\ ^2P_{3/2} \rightarrow 3s$ transition as a function of distance from the surface. It is seen that the emission intensity observed decreases near the surface, thus failing to show the density rise there. Using ray-tracing calculations [4], we verified that this resulted from the effects of self-absorption, limited spatial resolution, and low light collection efficiency near the surface that affect the spontaneous-emission measurements.

The population ratio of the $3s$ and $3p\ ^2P_{3/2}$ levels within $\simeq 30$ μm from the anode surface was found to be 2.8 ± 0.5. The uncertainty in the measured ratio results from the irreproducibility in the discharges, and from the uncertainty in the density ratio of the Mg II $3p\ ^2P_{3/2}$ and $3d$ levels, required for the determination of the population of the $3p\ ^2P_{3/2}$ level, as discussed in Sec. III A. The density ratio obtained agrees with that measured farther from the surface (given in Sec. III A), within the uncertainty of the measurements.

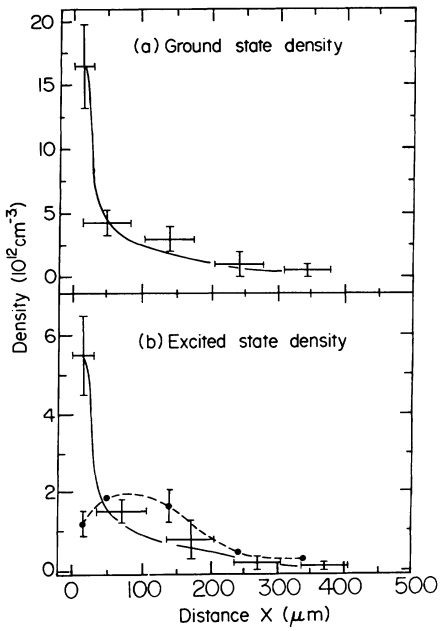

FIG. 7. (a) The Mg II ground-state density as a function of the distance x from the anode surface obtained from the laser absorption at 2795.5 Å for $t=55$ ns. The spatial resolution near the anode surface is $\simeq 30$ μm. The curve indicates the trend. The data reveal a large density gradient of the Mg II ground state near the anode surface. (b) Similar to (a) for the density of the Mg II excited state $3p\ ^2P_{3/2}$ obtained from the laser absorption at 2798 Å (solid curve), and the intensity of the $3p\ ^2P_{3/2} \rightarrow 3s$ emission in arbitrary units (dashed curve). The curves indicate the trends.

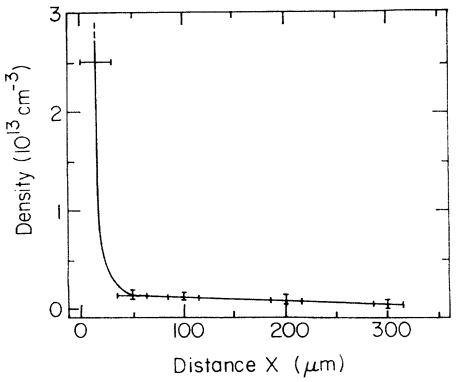

FIG. 8. The Li I ground-state density as a function of the distance x from the anode surface obtained from the laser absorption at 6708 Å ($2s \rightarrow 2p$) at $t = 70$ ns. The curve indicates the trend.

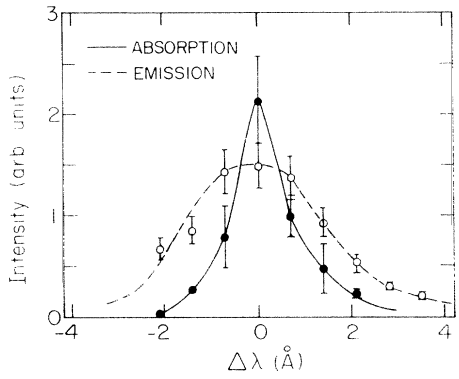

FIG. 10. Absorption and emission profiles of H_α for $t = 95$ ns obtained within $\simeq 50$ μm from the anode surface. The wavelength $\Delta\lambda$ is with respect to the line center. For the absorption, the laser wavelength was with a spectral width $\simeq 0.6$ Å, and was scanned over the line profile in different discharges. The emission profile was obtained in the same discharges.

Similar measurements were also performed for the Li I ground state using the $2s$-$2p$ line (6708 Å). The measured density of the Li I ground state as a function of distance from the anode surface is shown in Fig. 8. A density gradient higher than for Mg II was observed, the Li I density within 30 μm from the anode surface being > 20 times higher than farther away in the plasma.

Similar measurements were also performed for hydrogen, where we determined the $n = 2$ level density using the absorption of H_α. The results are shown in Fig. 9. Here the data point nearest to the surface is at $x = 50$ μm. Hydrogen is seen to be distributed much farther from the anode surface than Mg II and Li I.

The advantage of these absorption measurements near a surface over spontaneous emission measurements can also be demonstrated in the determination of line profiles, where line opacities are important. In Fig. 10 we present the H_α profile at $\simeq 50$ μm from the anode surface, obtained from the absorption measurements by scanning the laser wavelength in different discharges, together with the emission profile obtained in the same discharges. It is seen that the absorption profile is narrower than the emission profile, the σ_{FWHM}'s being $\simeq 1.1$ and 3.2 Å, respectively. Using the hydrogen $n = 2$ level density at $\simeq 50$ μm (given in Fig. 9), the emission light path in the plasma, and the absorption line spectral width, we estimate the optical depth at the line center to be $\simeq 8$. Accounting for the experimental uncertainties, our results are found to be consistent with an opacity broadening in the plasma, as estimated using the treatment given in Ref. [7]. Thus the absorption profile here obtained yields the true H_α profile, from which estimates on Doppler and Stark broadenings can be made (see Sec. IV).

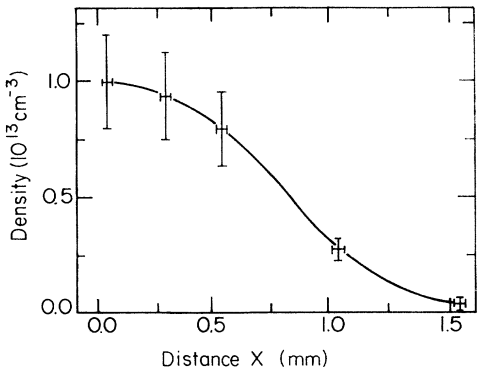

FIG. 9. The hydrogen $n = 2$ level density for $t = 95$ ns as a function of the distance x from the anode surface for $x \geq 50$ μm obtained from the H_α absorption. The curve indicates the trend. The laser wavelength is centered at $\lambda = 6562.8$ Å. The uncertainty in the absolute value is $\pm 50\%$ (not given in the figure), resulting mainly from the uncertainty in the shape of the spectral profile of the absorption line.

2. *The Mg II velocity distribution*

As described in Sec. III A, the observed spectral profile of the laser light transmitted through the plasma (as that shown in Fig. 4) was used to obtain the absorption line profile. The absorption line profile for the Mg II $3p\ ^2P_{3/2} \rightarrow 3s$ transition obtained within $\simeq 30$ μm from the anode surface is given in Fig. 11. This profile, dominated by Doppler broadening due to the relatively small Stark broadening for the density considered [3], yielded the Mg II velocity distribution parallel to the anode, giving a mean kinetic energy $\simeq 15$ eV within $\simeq 30$ μm from the anode surface. Similar kinetic energies were observed farther from the anode surface using the same measurements. We note that line shifts of 0–0.03 Å in opposite directions in different experiments were seen, but these shifts are too small to be important for the present discussion.

Velocity distributions of various ions in a similar anode plasma were observed by the use of spontaneous emission at distances $\gtrsim 200$ μm from the anode surface, as de-

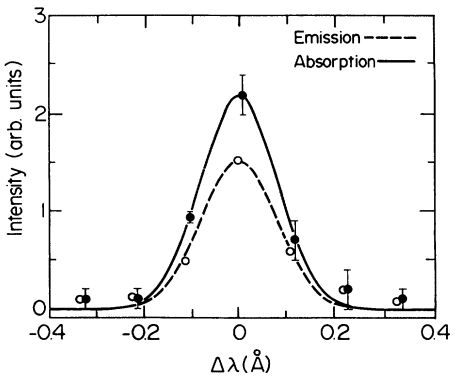

FIG. 11. Absorption and emission Doppler broadened profiles corresponding to the Mg II $3s-3p\ ^2P_{3/2}$ transition for $t=55$ ns obtained within $\simeq 30$ and $\simeq 100$ μm, respectively, from the anode surface. The wavelength $\Delta\lambda$ is with respect to the line center. The two profiles were measured in the same discharge. The uncertainty in each data point for the emission profile (not shown in the figure) is $\pm 15\%$. The two profiles give a temperature of $\simeq 15$ eV for Mg II. The lines are Gaussian fits to the data points.

scribed in Ref. [1]. The ion velocities normal to the anode surface were found to be similar to those parallel to it, giving a kinetic energy of $\simeq 20$ eV for the singly charged ions. One may therefore conclude that the velocities perpendicular to the surface within $\simeq 30$ μm from the surface are similar to those parallel to the surface observed in this region. Thus the similarity between the kinetic energies observed close to and farther from the surface means that the ions in the anode plasma acquire most of their kinetic energy within 30 μm from the anode surface, and that the average accelerating electric field in this region is $\simeq 5$ kV/cm.

3. *Discrimination against laser-light refraction in the plasma*

A major problem in resonant absorption measurements, in situations where high spatial resolutions are required and where high density gradients of the plasma particles that interact with the laser light occur, is the need to discriminate against the effect the light deflection out of the detection system due to refraction effects [8]. Here we show that such effects did not affect our present measurements. The density gradients here obtained from absorption by neglecting the refraction effects represent upper limits. Thus we use such gradients, as in Fig. 7, to estimate the maximum deflection angle due to resonant refraction. This was found to be much smaller than the light collection angle in our detection system (2.5 mrad), suggesting no significant refraction effects in our measurements. This was also consistent with the insensitivity to using various light collection angles found in the experiments.

Another support for the insignificance of the refraction in the present measurements can be found in Fig. 12. In Fig. 12(a) we give the absorption coefficient and the index of refraction of the Mg II $3s\rightarrow 3p\ ^2P_{3/2}$ transition, within 30 μm from the anode surface, obtained from the measurements described in Sec. III B. These parameters are used to calculate the spectral profile of the transmitted laser light for the two extreme cases, where the laser light only undergoes absorption in the Mg II layer or is only affected by refraction under the density gradient given in Fig. 7. In these calculations, the detection system geometry was modeled. The respective calculated profiles, given in Fig. 12(b), show the dip in the transmitted profile for the case of absorption and the two bumps in the profile for refraction. The latter results from the maximum and minimum in the refraction index shown in Fig. 12(a). We note that because of the small effect of the refraction and for the sake of demonstrating the effect of refraction on the profile, $(n-1)$ used to calculate the profile for refraction in Fig. 12(b) was exaggerated three times relative to that given in Fig. 12(a).

The observed profiles of the transmitted light for all transitions observed were found to be very similar to the profile calculated for absorption in Fig. 12(b), as shown in the example given in Fig. 4 for the Mg II $3s\rightarrow 3p\ ^2P_{3/2}$ transition. This demonstrates the predominance of absorption over refraction in our measurements, as assumed in the present study.

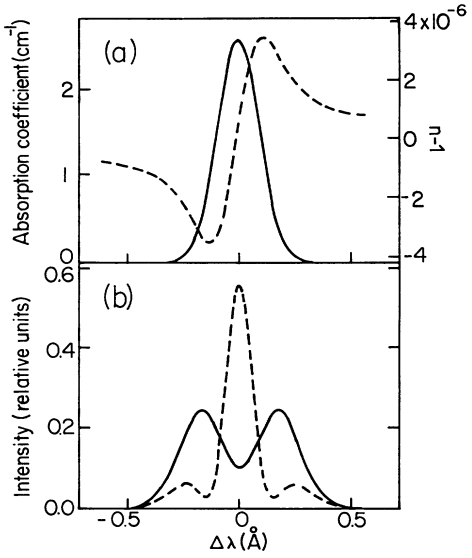

FIG. 12. (a) Calculated absorption coefficient (solid curve) and $n-1$ (dashed curve, n being the index of refraction) as a function of wavelength for the Doppler-broadened Mg II $3s\rightarrow 3p\ ^2P_{3/2}$ transition. For the calculations, the level densities within $\simeq 30$ μm from the anode surface given in Fig. 7, and the measured line profile given in Fig. 11, are used. The wavelength $\Delta\lambda$ is with respect to the line center. (b) Calculated spectral profiles of the transmitted laser light tuned to the center of the transition in (a) relative to the peak laser light intensity only for resonant absorption (solid curve) and only for deflections due to refraction (dashed curve). In the calculations, we used a Gaussian profile with $\sigma_{\mathrm{FWHM}}=0.32$ Å for the incident laser light. The effects of the light collection angle and of the spectral resolution of the detection system (0.11 Å) are accounted for.

IV. SUMMARY AND DISCUSSION

Techniques based on laser-light resonant absorption and induced fluorescence were developed to obtain high-spatial-resolution measurements of particle densities and velocities in plasmas near surfaces, and were implemented on the anode plasma in a magnetically insulated diode. In particular, the absorption measurements, that allow for direct determination of the ground-state density, were used to determine these parameters as a function of distance from the anode surface. With these measurements, these parameters averaged over a 30-μm-wide region near the surface were obtained.

Particle velocity distributions were determined from the Doppler broadened profiles of absorption lines. For Mg II, a kinetic energy $\simeq 15$ eV within $\simeq 30$ μm from the anode surface was observed. This is similar to the Mg II temperature observed at up to $\simeq 0.5$ mm from the anode surface. This shows that the Mg II velocities seen in the anode plasma are acquired by the ions within $\simeq 30$ μm from the anode surface. Electric fields of 5 kV/cm that accelerate ions off the surface in that region are consistent with the present results. This is a complement to our previous data [1,2], which suggested that the ion kinetic energies in the plasma result from the presence of electric fields at the immediate vicinity of the anode surface. Recently, a model for the ion acceleration near the anode surface was suggested [9]. It is based on the presence of nearly isotropic density gradients on a few tens of micrometers near the anode surface, where the ions are accelerated collisionlessly due to the density gradient of the collisional electrons.

The ratio between the Mg II ground state and the $3p\,^2P_{3/2}$ state densities obtained from the absorption and fluorescence measurements given in Sec. III A were found to be 3 ± 1 and 3.5 ± 1, respectively. The ratio calculated using our collisional-radiative code, that uses as input parameters the measured plasma electron density and temperature [1,10,11], was found to be 3.4. The agreement between the calculated and experimental ratios confirms the validity of the code calculations, and provides consistency with the independently determined electron density and temperature in the previous studies [1,10,11].

Densities of Li I, Mg II, and H I as a function of distance from the anode were obtained. Relatively high density gradients for L I and Mg II at distances of $\lesssim 50$ μm were observed, with the gradient for Li I being higher, while a significantly lower gradient was seen for H I, as given in Figs. 7, 8, and 9. We believe that the density gradients near the surface are significantly affected by the particle ionizations, with the higher gradients occurring for shorter ionization times and lower velocities of the particles as they move away from the surface. For example, the ionization times for H I, Mg II, and Li I calculated for $n_e = 1\times10^{15}$ cm^{-3} and $T_e = 10$ eV are $\simeq 80$, $\simeq 15$, and 3 ns, respectively, and their average axial velocities estimated from measured Doppler line widths are $\simeq 4$ cm/μsec [1] (8 eV), $\simeq 1$ cm/μsec ($\simeq 15$ eV), and 1.5 cm/μsec (8 eV), respectively. The propagation distances are therefore $\simeq 3$, $\simeq 0.15$, and $\simeq 0.05$ mm for H I, Mg II, and Li I, respectively, which is in a qualitative agreement with the gradients given in the figures.

The data here presented and a modeling of the ion flow were used to determine the electron density and temperature near the surface. In this modeling, we used collisional-radiative calculations to obtain the particle ionizations and level excitations as the particles move away from the anode surface as a function of time and distance x from the surface. The ion flow was assumed to be ballistic since for ions heavier than protons the Larmour radii are larger, and the collision times are longer than the distance and time of motion, respectively. Also in this modeling, we used the particle velocity distributions presently observed and the particle fluxes from the surface into the plasma determined in Ref. [2] for the neutral particles and ions.

The spatial distributions of the particle level-population densities, dependent on the electron density and temperature, were calculated for various values of these parameters. By fitting the calculated ground-state and excited-level spatial density distributions to the observed ones, this allowed bounds on the electron density and temperature within 50 μm from the anode surface to be obtained. An example of such fitting for the Mg II ground state is shown in Fig. 13. In this calculation we assumed $n_e = 1.3\times10^{15}$ cm^{-3} and $T_e = 10$ eV. The Mg II flux from the surface was assumed to be parabolic in time, $(t/38)-(-t^2/38^2)$, where t is in nanoseconds, as in Ref. [2]. For the velocity distribution in the x direction we used the positive half of the Mg II velocity distribution in the z direction determined from the Doppler broadened absorption profile given in Fig. 11.

In order to further limit the bounds on the electron density and temperature, similar measurements to those described in the above were performed to determine the C II $2s2p\,^2P_{3/2}$ level density as a function of distance from the surface. These measurements and a complete

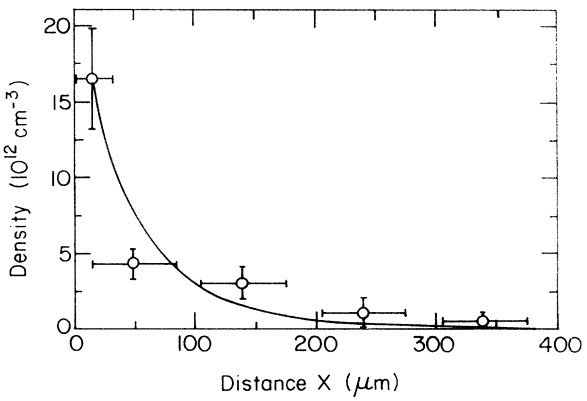

FIG. 13. The calculated (solid line) and measured (taken from Fig. 7) Mg II ground-state density as a function of the distance x from the anode surface. In the calculations, we assumed a ballistic ion flow away from the anode surface, $n_e = 1.3\times10^{15}$ cm^{-3}, $T_e = 10$ eV, and an Mg II source function parabolic in time [2]. The Mg II velocity distribution in the x direction is taken as the positive half of the velocity distribution observed in the z direction.

description of the modeling will be given in a later publication. Preliminary results of this modeling, using the measurements for H I, Li I, Mg II, and C II, give us bounds of 1×10^{15} to 3×10^{15} cm^{-3} for the electron density and a lower limit of 10 eV for the electron temperature, for the plasma region within 50 μm from the anode surface.

An upper bound for the electron density was also inferred from the contribution of the Stark broadening to the absorption H_α width given in Fig. 10 for the same location. For this inference, the contribution of the Doppler broadening, due to the few-eV temperature of H I previously observed [1] and the ion-dynamics effect on the H_α Stark profile [12], have been accounted for. The upper bound for the electron density thus obtained is found to be consistent with the value given above.

The electron density and temperature in the anode plasma farther away from the surface, at distances $\gtrsim 200$ μm, were observed to be $(1-2)\times10^{15}$ cm^{-3} [1,11] and $\simeq 10$ eV [10,11]. The results here obtained thus suggest that the electron density within 50 μm from the anode surface is similar to, and the electron temperature is at least, the respective parameters farther away from the surface.

A discussion of these findings in relation to a model [9] previously suggested to explain the nearly isotropic ion acceleration close to the surface will be made in the companion paper.

Our data also allow us to determine the absolute particle fluxes within 30 μm from the anode surface. Particle fluxes were also determined in our previous study [2] using spontaneous emission. However, since the spontaneous emission could not be collected efficiently from the $\simeq 150$-μm-wide region near the surface, those measurements gave the fluxes into the plasma at $\simeq 150$ μm from the surface. Thus, in order to compare the fluxes here obtained to the previous ones (for which data only on H I and Mg II are available), we first obtain from the present data the fluxes at $x = 150$ μm.

Using the measured H I $n=2$ level density at 150 μm from the anode surface, and collisional-radiative calculations with $n_e = 1\times10^{15}$ cm^{-3} and $T_e = 10$ eV, we obtain the total H I density to be $\simeq 1.3\times10^{15}$ cm^{-3}. Together with the H I velocity in this region (4 cm/μs) [1], this gives $\simeq 5\times10^{12}$ cm^{-2} ns^{-1} for the H I flux, which agrees to within a factor of 2 with the flux reported in Ref. [2], i.e., to within the uncertainties stated for the two measurements.

In order to compare the Mg II flux, we first note that the amount of the MgF_2 used in the epoxy anode in the present experiments was four times larger than in the previous experiments. Thus the presently obtained Mg II flux at 150 μm from the surface should be reduced by a factor of 4 when compared to Ref. [2]. The Mg II flux at 150 μm determined as in the above for hydrogen is 6.5×10^{9} cm^{-2} ns^{-1}, which, after accounting for this factor, is in agreement to within a factor of 2 with that given in Ref. [2] (7.8×10^{8} cm^{-2} ns^{-1}).

We now give the fluxes averaged over $\simeq 30$ μm from the surface, obtained from the densities and velocities measured here. These fluxes are $\simeq 5\times10^{12}$, $\gtrsim 6\times10^{10}$, and $\simeq 3.5\times10^{10}$ cm^{-2} ns^{-1} for H I, Li I, and Mg II, respectively. The H I flux given above is similar to that at 150 μm, since ionization effects for H I in this region are negligible. However, the fluxes of the fast-ionizing particles Li I and Mg II are much higher at 30 μm than at 150 μm. This demonstrates the need to measure the charge-state distributions as close as possible to the surface in order to improve our knowledge of the processes at the immediate vicinity of the surface.

We believe that measurements similar to those described in this paper can be useful in studying various phenomena near a plasma-wall interface.

ACKNOWLEDGMENTS

The authors are grateful to A. Fisher and A. E. Blaugrund for reading the manuscript, and to A. Fruchtman and E. Braun for critical discussions. Thanks are due to E. Elias for help in the data analysis and to P. Meiri, Y. Danino, and Y. Macaby for skilled technical assistance.

[1] Y. Maron, E. Sarid, O. Zahavi, L. Perelmutter, and M. Sarfaty, Phys. Rev. A **39**, 5842 (1989).

[2] Y. Maron, L. Perelmutter, E. Sarid, M. E. Foord, and M. Sarfaty, Phys. Rev. A **41**, 1074 (1990).

[3] H. Griem, *Plasma Spectroscopy* (McGraw-Hill, New York, 1964).

[4] L. Perelmutter, G. Davara, and Y. Maron, Bull. Am. Phys. Soc. **35**, 2120 (1990).

[5] C. Mendoza, J. Phys. B **14**, 2465 (1981); Yu. Ralchenko (private communication).

[6] L. Perelmutter, Ph.D. thesis, Weizmann Institute of Sciences, Rehovot, Israel, 1991.

[7] J. Richter, in *Plasma Diagnostics,* edited by W. Lochte (North-Holland, Amsterdam, 1968).

[8] L. D. Landau and E. M. Lifshits, *Electrodynamics of Continuous Media,* 2nd ed. (Pergamon, Oxford, 1984), pp. 290–293.

[9] R. E. Duvall, A. Fruchtman, Y. Maron, and L. Perelmutter, Phys. Fluids B **5**, 3399 (1993).

[10] Y. Maron, M. Sarfaty, L. Perelmutter, O. Zahavi, M. E. Foord, and E. Sarid, Phys. Rev. A **40**, 3240 (1989).

[11] E. Sarid, Y. Maron, and I. Troyansky, Phys. Rev. E **48**, 1364 (1993).

[12] S. Alexiou (private communication).